Supplementary Information

Anisotropic Kinetics of Solid Phase Transition from First Principles: Alpha-Omega Phase Transformation of Zr

Shu-Hui Guan, Zhi-Pan Liu*

Collaborative Innovation Center of Chemistry for Energy Material, Key Laboratory of Computational Physical Science (Ministry of Education), Shanghai Key Laboratory of Molecular Catalysis and Innovative Materials, Department of Chemistry, Fudan University, Shanghai 200433, China

Part 1. The α-ω crystallographic orientation relationships in literatures

Table SI The orientation relations (OR) for α-ω phase transition in literatures (not limited to Zr).

	Conditions	Variant-I OR	Variant-II OR
J. M. Silcock[1] (Silcock) 1958	TiV, TiMo and TiCr alloys; XRD		$(0001)\alpha\|\|(11\bar{2}0)\omega$; $[1\,\bar{2}\,0]\alpha\|\|[0001]\omega$ (**Silcock OR = UZ Variant-II OR**)
M. P. Usikov and V. A. Zilbershtei[1] (UZ) 1973	Zr, Ti under static pressure (10 GPa); Theory and TEM	$(0001)\alpha//(01\bar{1}1)\omega$; $[11\bar{2}0]\alpha//[10\bar{1}1]\omega$ (observed in experiment)	$(0001)\alpha//(11\bar{2}0)\omega$; $[11\bar{2}0]\alpha//[0001]\omega$ (not observed in experiment)
A. Rabinkin, M. Talianker and O. Botstein [2](RTB) 1980	Zr under static pressure (6 GPa); high resolution dark-field electron microscopy and selected area diffraction(SAD)		$(0001)\alpha//(1\bar{2}10)\omega$; $[\bar{2}110]\alpha//[0001]\omega$ variant1 $(0001)\alpha//(1\bar{2}10)\omega$; $[\bar{1}\bar{1}20]\alpha//[0001]\omega$ variant2 $(0001)\alpha//(1\bar{2}10)\omega$; $[\bar{1}2\bar{1}0]\alpha//[0001]\omega$ variant3 (**RTB OR=UZ Variant-II OR**)
Kutsar et al [3]1990	Shock samples Zr (8-32 GPa) Reverse ω→α; XRD, TEM		$(0001)\alpha//(11\bar{2}0)\omega$; $[\bar{1}\bar{1}20]\alpha//[0001]\omega$
S. Song and G. T. Gray[4] (SG) 1995	Zr shock-loaded (7 GPa); SAD,TEM	$(0001)\alpha//(10\bar{1}1)\omega$; $[10\bar{1}0]\alpha//[11\bar{2}\bar{3}]\omega$ (**SG = UZ Variant-I OR**)	
G. Jyoti, K.D. Joshi , Satish C. Gupta,Sikka SK 1997[5]	Shock-loaded Zr (11.8GPa) SAD,TEM	UZ ORI, also SG	
D. R. Trinkle, R.G. Hennig and J.W.Wilkins [6] 2003	Ti Theory	$(0001)\alpha//(0\bar{1}11)\omega$; $[11\bar{2}0]\alpha//[01\bar{1}1]\omega$ (**TAO-1= UZ Variant-I OR**)	
G.T. Gray[7] 2005	Highest purity Zr under static pressure (7.1-8 GPa); SEM, TEM	$(0001)\alpha//(\bar{1}101)\omega$; $[\bar{1}010]\alpha//[\bar{2}11\bar{3}]\omega$	
Jyoti G 2008[8]	Shock compressed Zr (11.6	Confirm UZ	

	GPa) TEM, XRD, SAD	Variant-I OR	
Wenk Kaercher [9] 2013	Zr D-DIA and DAC at 1.5-4.5 GPa; *in situ* synchrotron x-ray diffraction;		(0001)α//(11$\bar{2}$0)ω; [11$\bar{2}$0]α//[0001]ω; highly reversible
Zong , Lookman[10] 2014	Anisotropic shock response of Ti using molecular dynamics (Theory)	Shock along [0001]α (0001)α//(10$\bar{1}$0)ω; [10$\bar{1}$0]α//[11$\bar{2}$3]ω	Shock along [10$\bar{1}$0]α and [1$\bar{2}$10]α (0001)α//(11$\bar{2}$0)ω; [11$\bar{2}$0]α//[0001]ω
Zong , Lookman[11] 2014	Zr Ti 15-20 μm, shock at 8 GPa recovered samples ω→α XRD		(0001)α//(11$\bar{2}$0)ω; [11$\bar{2}$0]α//[0001]ω Reversibility, Heterogeneous nucleation observed

Part 2 Theoretical methods

a. Stochastic Surface Walking (SSW) pathway sampling

The SSW methodology has been described in our previous work in detail[12, 13]. We have shown that the SSW method is able to explore the potential energy surface (PES) to identify unexpected new structures, including clusters and crystals, and at the mean time to collect the reaction pathways leading to them. This is attributed to the fact that SSW PES searching involves generally small displacement on lattice and atoms, and thus the pathway information is maintained from one minimum to another.

The purpose of SSW crystal pathway sampling is to establish a one-to-one correspondence for lattice ($L(e_1,e_2,e_3)$, e_i being the lattice vector) and atom (q_i, i=1,..3N, N is the number of atom in cell) from one phase to another. The lattice here does not necessarily be the conventional Bravais lattice but any possible set of lattice that describe the same crystal phase. Using such a pair of coordinates, $Q_{IS}(L,q)$ and $Q_{FS}(L,q)$ (IS and FS are the initial and the final states), it is then possible to utilize double-ended transition state searching method to identify the reaction pathway and the transition state. The current approach is different from the traditional Landau-type theory where the lattice correspondence needs to be assumed. The procedure is described below briefly.

Pathway collection In SSW pathway sampling, firstly, we start from one single phase (starting phase), and utilize the SSW method to explore all the likely phases nearby the phase. A structure selection module is utilized to decide whether to accept/refuse once a new minimum is reached. If the new phase different from the starting phase is identified by the SSW crystal method[14], we record/output the IS (i.e. starting phase) and the FS (a new phase) of the current SSW step. Then, the program will return back to the IS by rejecting the new minimum to continue the phase exploration; On the other hand, if the new minimum identified by SSW is still the starting phase (e.g. the same symmetry but a permutation isomer with varied lattice), the program will accept the new isomeric phase and start the phase exploration from this phase. We repeat this procedure until a certain number of IS/FS pairs are reached.

Pathway screening Secondly, we utilize the variable-cell double-ended surface walking (DESW) method[15] to establish the pseudopathway connecting IS to FS for all IS/FS pairs [16, 17]. The approximate barrier is obtained according to DESW pseudopathway, where the maximum energy point along the pathway is generally a good estimate for the true TS [15]. By sorting the approximate barrier height, we can obtain the candidates for lowest energy pathways.

It might be mentioned that at this stage, we generally examined thoroughly all the pathways we identified. Basically, even before we locate exactly the TS, we can have the following important information, including the approximate barrier, the pattern of lattice and atom movement from IS to FS, the atomic habit plane and the OR for the pathways, From these, we can safely rule out the similar pathways and focus on the selected,

distinct and low energy pathways.

Lowest energy pathway determination Thirdly, the candidate lowest energy pathways are selected to locate exactly the "true" TS by using DESW TS-search method[15]. By sorting the exact barrier calculated, the energy difference between the TS and the IS, the lowest energy pathways can be finally obtained. All the lowest energy pathways will be further confirmed by extrapolating TS towards IS and FS, and the TSs are validated by phonon spectrum calculation, showing one and only one imaginary mode.

For α-ω phase transition in this work, starting either from α or ω phase, the DFT-based SSW pathway sampling in the 6-atom cell simulation visits 5777 minima nearby IS (see PES shown in Figure 2a) and collects 233 IS/FS pairs (see Figure S1 below); in the 12-atom cell simulation, visits 2193 minima and collects 33 IS/FS pairs. All the calculations were performed under 3 GPa hydrostatic pressure.

Figure S1 plots the structure of high-symmetry Zr crystal phases obtained from SSW sampling. We can identify all the common phases, including the simple hexagonal phase (ω, the global minimum at 3 GPa), the α phase, the body-center cubic (bcc, no. 229), and also other possible phases, such as face-center cubic (fcc, no.225) and a cubic phase (no.139). These phases can be distinguished by their symmetry, the volume and the coordination of Zr. In this work, the coordination is defined as Eq. S1 below

$$C = \frac{C_0}{N_0} \sum_{i=1}^{N_0} \sum_{j=1(i\neq j)}^{N} \frac{1}{1+e^{d_{ij}-d_0}} \qquad \text{(S1)}$$

where N_0 is the number of Zr atoms in the primitive cell and N is the number of Zr atoms in the supercell ((3x3x3) of the primitive cell), i and j are the label of atom; d_{ij} is the distance between the i atom and j atom; d_0 is a constant being 3.24 (Å); C_0 is a scaling constant being 1.33 to yield ~12-coordination for Zr in α phase.

Figure S1 plots the approximate barrier from DESW peudopathways against the scaled Euclidean distance of the pathway for α-ω phase transitions. It includes the results from both 6-atom and 12-atom sampling. In the 6-atom sampling, 51 of 233 pathways have the approximate barrier below 90 meV/atom with respect to α phase. Among them, 13 lowest energy pathways in the bottom left corner were selected for the exact TS location. This leads to the finding of the lowest energy pathways, **P-I to P-IV** (see Figure 1b and also Figure S1). In the 12-atom sampling, 16 of 37 pathways have the approximate barrier below 90 meV/atom with respect to α phase. Among them, 12 lowest energy pathways in the bottom left corner were selected for the exact TS location. This leads to the finding of the same lowest energy pathways, **P-I** and **P-II**.

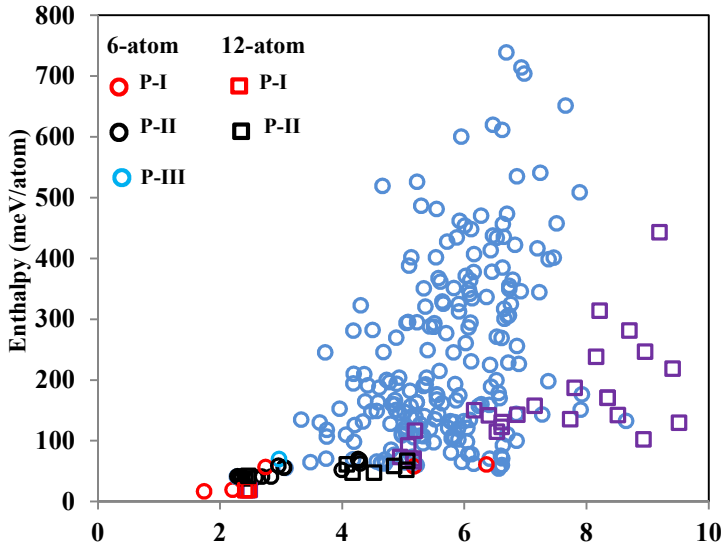

Figure S1. Pathway screening by plotting the approximate energy barrier (eV/6-atom with respect to α phase) versus the scaled Euclidean distance (Å) between two phases (measured from the pathways) under 3 GPa. In

total, there are 233 pathways from 6-atom sampling and 37 pathways from 12-atom sampling. The approximate barrier is obtained according to DESW pseudopathway, where the maximum energy point along the pathway is generally a good estimate for the true TS [15]. Only the lowest energy pathways, **P-I** to **P-III** are highlighted.

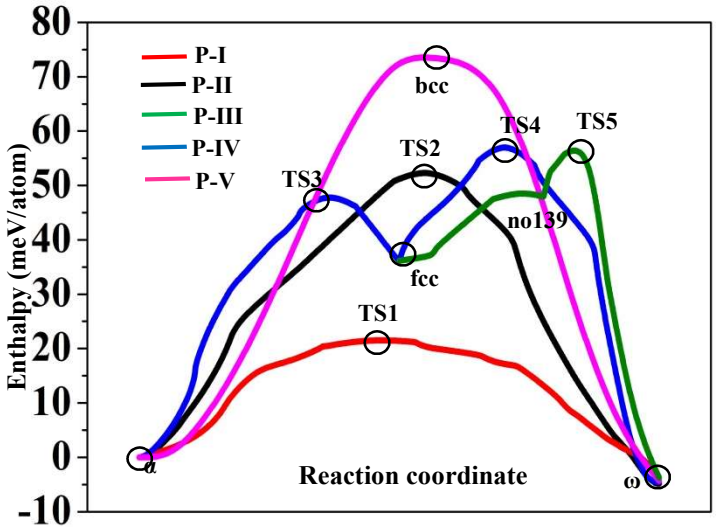

Figure S2 Potential energy profile for five lowest energy pathways for α-ω solid phase transition, **P-I** to **P-V** (**P-I** to **P-III** are also discussed in the text).

b. DFT calculation details

All calculations were perfomed using the plane wave DFT program, Vienna ab initio simulation package VASP [18, 19] where Zr electron-ion interaction was represented by the projector augmented wave (PAW)[20] and the exchange-correlation functional utilized was GGA-PBE[21]. In the pathway sampling, we adopt the following setups to speed up the PES exploration: plane-wave cutoff 400 eV; the Monkhorst-Pack k-point mesh of (6×6×6) set for 6-atom supercell and (4×4×4) set for 12-atom supercell; 4-electron (4d5s5p) PAW pesudopotential for Zr. To obtain accurate energetics for the pathways, a more accurate calculation setup was utilized: the plane-wave cutoff 600 eV; the k-point mesh up to (10×10×10) set and 12-electron (4s4p4d5s5p) PAW pesudopotential for Zr. For all the structures, both lattice and atomic positions were fully optimized until the maximal stress component is below 0.1 GPa and the maximal force component below 0.001 eV/Å, which leads to the convergence of the relative energy (e.g. barrier) below 2 meV/atom. The convergence of the energetics with respect to k-point mesh is shown in Table SII.

TABLE SII The convergence of energetics (meV/atom) for the key states (6-atom cell, see **Part 6** for structures) in **P-II** with respect to different k-point mesh. The energy of α-phase is set as zero reference. The TS has been re-optimized under each k-point set.

k-point mesh	6×4×6	8×6×8	8×8×8	10×8×10
α phase	0	0	0	0
TS2	51.58	53.67	53.27	51.62
ω phase	-2.31	-4.84	-4.94	-4.71

c. Phonon and elastic properties

The phonon frequencies of the crystals were determined using the finite displacement method[22, 23], employing the PHONOPY package [24]. In these calculations, the size of the system was increased to (2×2×2) supercell (48-atom supercell) and the K-point utilized is (2×2×2) Monkhorst-Pack mesh. With a displacement of ±0.01 Å on nonequivalent atoms, a set of displaced supercells was generated and the forces

of these supercells were calculated using plane-wave DFT package, VASP program. These forces were carried back to the PHONOPY to calculate the phonon dispersion curves. The TS phonon spectra are shown in Figure S4, confirming one and only one negative phonon mode in the Brillion zone for the TS obtained in this work.

The elastic tensor is determined by performing six finite distortions of the lattice and deriving the elastic constants from the strain-stress relationship[25]. The linear elastic constants C_{ij} from a 6×6 symmetric matrix, have 27 different components, fulfilling $\sigma_i = C_{ij}\varepsilon_j$ for small stresses σ and strains ε values[26]. Properties such as the bulk modulus, shear modulus can be computed from C_{ij}.

Specifically, the bulk modulus (B) and shear modulus (G) can be estimated from the individual elastic constants C_{ij} by the Voigt approximation and the Reuss approximation[27, 28]. The expressions for the Voigt and Reuss approaches are represented in Eqs. (S2-3) for bulk and shear modulus:

$$B_v = \frac{1}{9}(C_{11}+C_{22}+C_{33}) + \frac{2}{9}(C_{12}+C_{23}+C_{13}) \quad \text{(S2)}$$

$$G_v = \frac{1}{15}(C_{11}+C_{22}+C_{33}) - \frac{1}{15}(C_{12}+C_{23}+C_{13}) + \frac{1}{5}(C_{44}+C_{55}+C_{66}) \quad \text{(S3)}$$

Part 3. Pressure dependence of homogeneous phase transition pathways (P-I and P-II)

To understand the pressure dependence of the α-ω solid phase transition, we have also calculated the enthalpy barrier of the lowest energy homogeneous phase transition pathways, P-I and P-II, under different pressure conditions. The results are shown in Figure S3. We found that the barrier of P-I changes slightly with the change of the pressure, while the barrier of P-II decreases quite rapidly with the increase of the pressure. Nevertheless, the barrier of P-II is always higher than that of P-I at the interested pressure regions, even at the high pressures, e.g. 12 GPa. This indicates that P-I is always the preferred homogeneous phase transition channels that could be responsible for the initial nucleation events. Therefore, the observation on two different ORs in experiment cannot be attributed to the homogeneous phase transition mechanism alone. In the main text, we have shown in Figure 3 that it is the heterogeneous phase propagation pathways that are responsible for the pressure dependence of α-ω solid phase transition observed in experiment.

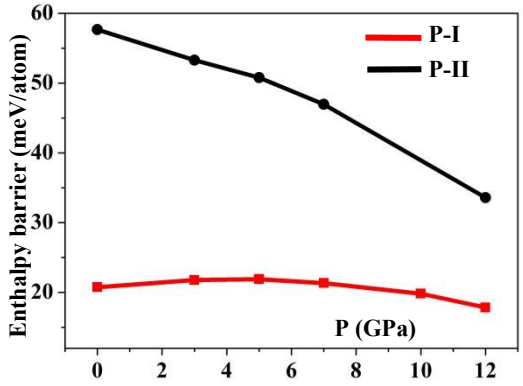

Figure S3. DFT enthalpy barrier with respect to α phase as a function of hydrostatic pressure for the homogeneous transition pathways P-I and P-II.

Part 4. Numerical search to determine the OR and search for atomic habit planes (coherent interface)

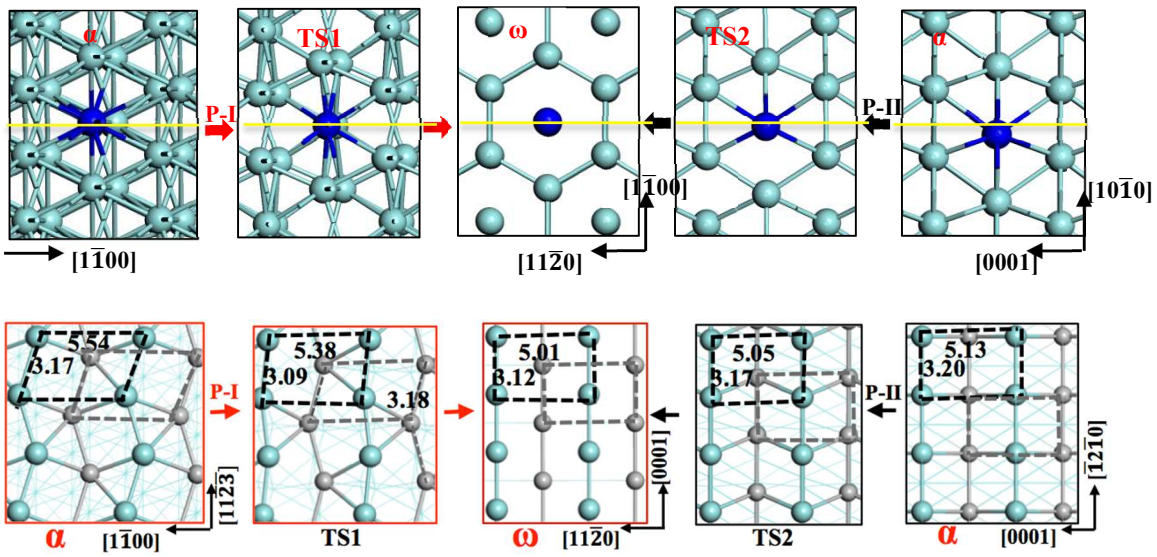

Figure S4. Snapshots for α-ω transformation in the homogeneous phase transition pathways, **P-I and P-II**. In the top panel are the views from $[0001]_\omega$ direction. Yellow lines are the atomic habit plane edge. The blue atoms highlights the atom row with zero displacement at $[0001]_\omega$ during the phase transition. Those in the bottom panel highlight the atom displacement viewed down from the determined atomic habit plane, $(11\bar{2}2)_\alpha$ (P-I) and $(10\bar{1}0)_\alpha$ (P-II). The distances labeled are in Å. Cyan and Grey: Zr at two different layers.

The SSW pathway sampling provides the lowest energy pathway between two connecting phases, which determines the lattice and atom correspondence, as illustrated in Figure S4 for α-ω phase transition in **P-I** and **P-II**. The lattice parameters and atomic coordinates of **P-II** utilized in the following analysis are provided in **Part 6**. Note that the lattice and atom coordinates identified in the lowest pathways are generally not in conventional Bravais lattice of crystal. In the following, we describe in detail the three steps that are required to identify the atomic habit plane (coherent interface) between two phases.

Step1: Determine Strain Invariant (minimum) Planes

Based on the lattice correspondence, we can first use the classical phenomenological theory of Martensitic crystallography (PTMC) [29-35] to determine the invariant line strain, the possible habit planes and ORs.

Determine the principal axes of the phase transformation.

Let define two lattices as **T** and **M,** both (3x3) matrix of lattice.

A deformation gradient **F** matrix transform an initial lattice **T** to a final lattice **M**, as

$$\mathbf{FT= RBT=M}$$

$$\mathbf{F=RB}$$

where R is a rigid-body rotation matrix and B is a lattice deformation matrix, representing the generalized Bain deformation. In PTMC, **F** is also known as a homogeneous *invariant line strain*.

The Gauchy-Green deformation tensor is

$$\mathbf{C=F^TF=(T^T)^{-1}\,M^T\,MT^{-1}}$$

C is rotational invariant.

The principal axes are the eigenvectors ($\mathbf{e_i}$, i=1,2,3) of the Gauchy-Green deformation tensor

$$\mathbf{Ce_i= l_ie_i}$$

The strain energy of the lattice deformation is defined the sum of three eigenvalues, $\mathbf{l_i}$

$$I=\mathrm{tr}(\mathbf{F^TF})= \mathbf{l_1+ l_2+l_3}$$

Taking **P-II** in α-ω phase transition as the example (which is simpler because its Martensitic mechanism), three principal axes (Cartesian coordinate) are as follows using α-phase as initial phase and ω-phase as final phase:

e_1: (0.0084 0.6913 -0.7225)$_\alpha$; **l_1**= 0.83077

e_2: (1.0000 -0.0049 0.0070)$_\alpha$; **l_2**= 0.95218

$\mathbf{e}_3$: $(-0.0013 \quad 0.7226 \quad 0.6913)_\alpha$; $\mathbf{l}_3 = 1.23703$

Obviously, $\mathbf{e}_2$ direction is the principal axes with the lowest strain.

Determine the strain invariant lines (SIL) and strain invariant planes (SIP)

For Martensitic phase transition, three eigenvalues of matrix **C** could not be all larger than one or all smaller than 1 and in general $\mathbf{l}_2$ should be close to unity for generating SIP (otherwise only strain minimum planes can be obtained):,

$$\mathbf{l}_1 < 1; \mathbf{l}_2 > 1; \mathbf{l}_3 > 1; \quad \text{or} \quad \mathbf{l}_1 < 1; \mathbf{l}_2 < 1; \mathbf{l}_3 > 1 \quad (\mathbf{l}_3 > \mathbf{l}_2 > \mathbf{l}_1)$$

Using three eigenvectors **e** as the basis, we need to determine the strain invariant lines on a corn surrounding the maximum or the smallest $\mathbf{e}_i$. This is equivalent to find the fractional coordinate (a,b,c) in the following two equations.

$$a^2+b^2+c^2=1$$
$$a^2\,\mathbf{l}_1+b^2\,\mathbf{l}_2+c^2\,\mathbf{l}_3=1$$

While there are in principle infinite number of solutions for (a,b,c), the problem can be simplified by identifying the strain invariant lines on the plane defined by the largest and the smallest eigenvectors, $\mathbf{e}_1$ and $\mathbf{e}_3$., i.e. by setting

$$b=0$$

These strain invariant lines can thus be solved as

$$\boldsymbol{sil}_1 = a\mathbf{e}_1 + c\mathbf{e}_3 \text{ and } \boldsymbol{sil}_2 = a\mathbf{e}_1 - c\mathbf{e}_3$$

In **P-II** of α-ω phase transition, two solutions of ***sil*** (Cartesian coordinate) vector on the plane with $\mathbf{e}_1 \times \mathbf{e}_3$ normal are yielded:

***sil*$_1$:** $(0.0056 \quad 0.9944 \quad -0.1057)_\alpha$
***sil*$_2$:** $(-0.0073 \quad -0.0617 \quad 0.9981)_\alpha$

Similarly, the SILs on the plane defined by $\mathbf{e}_2$ and $\mathbf{e}_3$ can be found (in these cases, a nonzero strain on the principal axis $\mathbf{e}_1$ will be considered in the following step to generate strain minimum planes):

***sil*$_3$:** $(0.9116 \quad 0.2916 \quad 0.2896)_\alpha$
***sil*$_4$:** $(-0.9127 \quad 0.3005 \quad 0.2768)_\alpha$

Using a ***sil*** vector and another untilted line, e.g. the principal axes **e** normal to ***sil***, it is possible to construct the so-called strain invariant (minimum) plane, the habit plane. All lines on habit plane are unrotated, which should contain a strain invariant line and also an untilted line. These lines and their angle are unchanged under the rigid-body rotation and the lattice deformation. The habit plane normal ***sip***, a unit vector, can be solved using

$$\boldsymbol{sip}_k = \boldsymbol{sil}_i \times \mathbf{e}_j$$
$$\mathbf{F}\,\boldsymbol{sip}_k = \mathbf{RB}\,\boldsymbol{sip}_k = \boldsymbol{sip}_k$$

In **P-II** of α-ω phase transition, two solutions of $\boldsymbol{sip}_i$, i=1, 2 with the minimum strain are yielded. In the convention of Miller plane, ***sip*** are named using (hkl) with real numbers:

***sip*$_1$:** $(0.0332 \quad -0.8978 \quad -3.0609)_\alpha$ $\quad \boldsymbol{sip}_1 = \boldsymbol{sil}_1 \times \mathbf{e}_1$
***sip*$_2$:** $(0.0227 \quad 8.4727 \quad -0.4164)_\alpha$ $\quad \boldsymbol{sip}_2 = \boldsymbol{sil}_2 \times \mathbf{e}_1$

The second lowest strain planes based on $\mathbf{e}_2$ can be similarly derived:

***sip*$_3$:** $(-2.1084 \quad 5.6087 \quad 1.5698)_\alpha$ $\quad \boldsymbol{sip}_3 = \boldsymbol{sil}_3 \times \mathbf{e}_2$
***sip*$_4$:** $(-2.0960 \quad -5.582 \quad -1.5885)_\alpha$ $\quad \boldsymbol{sip}_4 = \boldsymbol{sil}_4 \times \mathbf{e}_2$

Step 2: Determine the crystal planes with minimum strain and minimum atomic movement

Now we need to go beyond PTMC by considering the atomic movement in the phase transition.
The possible $\boldsymbol{sip}_i$ only takes into account the lattice strain between two connecting phases but the atomic

match at the interface cannot be quantitatively measured. For diffusionless Martensitic phase transition, it is important that the atoms at the phase junction are closely matched and thus the atomic displacement needs to be as small as possible from one phase to another.

Based on the atom correspondence from the pathway obtained from SSW, we can search for the crystal plane with minimum strain and minimum atomic movement.

a. The minimum strain condition is first utilized to screen the possible crystal Miller planes by minimizing the dihedral angle between the crystal plane ((hkl) with integer number) and the $\boldsymbol{sip_i}$.
b. The atomic movement can be calculated by summing the displacement of each atom from initial to the final phase while projecting out those due to rigid-body rotation.

The atomic movement is composed of two types of movement, parallel to the crystal plane (hkl) and perpendicular to the plane, $\mathbf{d}^{\perp}$. For Martensitic phase transition, the phase transition is achieved often via slipping or twinning and thus the atomic movement needs to be dominated by those parallel to the habit plane.

In **P-II** of α-ω phase transition, if limiting the search within low index planes **(hkl)** with the absolute value of h, k, l being 0 or 1. Two solutions corresponding to $\boldsymbol{sip_i}$, i=1, 2 are yielded:

SOLUTION 1: $(001)_\alpha$ plane, which is 9.08 degrees (**angle**) off $\boldsymbol{sip_1}$. The atomic movement is 1.80 Å parallel to the plane and 2.80 Å perpendicular to the plane ($\mathbf{d}^{\perp}$).

SOLUTION 2: $(010)_\alpha$ plane, which is 7.48 degrees off $\boldsymbol{sip_2}$. The atomic movement is 2.94 Å parallel to the plane and 1.36 Å perpendicular to the plane.

The **SOLUTION 2**, $(010)_\alpha$ has the smallest $\mathbf{d}^{\perp}$ (1.36 Å). By switching to the notation in conventional Bravais lattice, $(010)_\alpha$ is $\mathbf{(1\bar{1}00)_\alpha}$

The solutions for the second lowest strain planes are as follows:

SOLUTION 3: $(\bar{1}11)_\alpha$ plane, which is 24.84 degrees off $\boldsymbol{sip_3}$. The atomic movement is 2.66 Å parallel to the plane and 2.04 Å perpendicular to the plane.

SOLUTION 4: $(111)_\alpha$ plane, which is 24.56 degrees off $\boldsymbol{sip_4}$. The atomic movement is 2.66 Å parallel to the plane and 2.04 Å perpendicular to the plane.

We note that $(\bar{1}11)_\alpha$ and $(111)_\alpha$ are the same plane for α phase in the lattice of P-II. By switching to the notation in conventional Bravais lattice, $(111)_\alpha$ is $\mathbf{(1\bar{1}01)_\alpha}$

Step 3: Identify the atomic habit plane (interface)

Finally, we utilize the determined possible atomic habit planes to establish the interface between two phases (see Figure S4). An atomic habit plane needs to exhibit a coherent interface between two phases, i.e. with the lowest interfacial energy.

For **P-II** in α-ω phase transition, we have two likely interfaces as suggested from Step 2: $(10\bar{1}0)_\alpha$ //$(1\bar{1}00)_\omega$ and $(1\bar{1}01)_\alpha$//$(01\bar{1}1)_\omega$. $(10\bar{1}0)_\alpha$//$(10\bar{1}0)_\omega$ has both minimum strain and minimum $d^{\perp}$. By manually joining the two surfaces of the two phase together, we found that $(10\bar{1}0)_\alpha$//$(1\bar{1}00)_\omega$ pair can form a coherent interface between the two phases. The DFT optimized interface is shown in the Figure S5 (d) with a low interfacial energy, 4 meV/Å^2. We therefore conclude that $(10\bar{1}0)_\alpha$//$(1\bar{1}00)_\omega$ is the atomic habit plane and the OR can be written as $(10\bar{1}0)_\alpha$//$(1\bar{1}00)_\omega$; $[0001]_\alpha$//$[11\bar{2}0]_\omega$, which is equivalent to UZ Variant-II OR in literature.

Using the same approach, the OR and atomic planes (HP) for **P-I** could also be established. The **e**, **I** and ***sil*** and ***sip*** as defined in **Part 4** are listed in Table SIII below. Unlike that in **P-II**, we found that $\boldsymbol{sip_1}$ and $\boldsymbol{sip_2}$ have minimum strain but with large $d^{\perp}$, but $\boldsymbol{sip_3}$ and $\boldsymbol{sip_4}$ has a larger strain but with small $\mathbf{d}^{\perp}$. In particular, $\boldsymbol{sip_4}$ has a diminished $d^{\perp}$**.** By constructing these interfaces involving $\boldsymbol{sip_4}$ and $\boldsymbol{sip_2}$ in the superlattice, namely, $(11\bar{2}2)_\alpha$//$(1\bar{1}00)_\omega$ and $(\bar{1}2\bar{1}1)_\alpha$//$(1\bar{1}00)_\omega$, we found that $(11\bar{2}2)_\alpha$//$(1\bar{1}00)_\omega$ from $\boldsymbol{sip_4}$ can achieve a stable

interface, while the $(\bar{1}2\bar{1}1)_\alpha//(1\bar{1}00)_\omega$ from ***sip*$_2$** is not stable, the optimization of which leads to pure phase. The structure of these interfaces are shown in Figure S5. The atomic habit plane is therefore determined as $(11\bar{2}2)_\alpha//(1\bar{1}00)_\omega$ with OR as $(11\bar{2}2)_\alpha//(1\bar{1}00)_\omega$; $[1\bar{1}00]_\alpha//[11\bar{2}0]_\omega$, which is equivalent to UZ Variant-I OR in literature.

Table SIII. The OR and atomic habit planes (HP) for **P-I** (the structures are listed in **Part 7**). The **e**, **I**, ***sil*** and ***sip*** are as defined in **Part 4**.

P-I		Note
$\mathbf{e}_1$	(0.4200 -0.3419 -0.8407)	
$\mathbf{e}_2$	(0.8878 0.3471 0.3024)	
$\mathbf{e}_3$	(0.1884 -0.8733 0.4492)	
$\mathbf{I}_1$	0.80745	
$\mathbf{I}_2$	0.97747	
$\mathbf{I}_3$	1.23083	
***sil*$_1$**	(0.4371 -0.8414 -0.3178)	(on the plane defined by) $\mathbf{e}_1\times\mathbf{e}_3$
***sil*$_2$**	(-0.183 -0.3365 0.9237)	$\mathbf{e}_1\times\mathbf{e}_3$
***sil*$_3$**	(0.9036 0.0708 0.4226)	$\mathbf{e}_2\times\mathbf{e}_3$
***sil*$_4$**	(-0.7912 -0.5917 -0.1546)	$\mathbf{e}_2\times\mathbf{e}_3$
		***(hkl) angle $d^{\perp}$**
***sip*$_1$**	(-0.8684 -1.6743 5.4062)	(001) 26.0° 2.3325
***sip*$_2$**	(-2.5451 5.3912 -1.6406)	$(1\bar{1}0)$ 28.73° 2.3230
***sip*$_3$**	(0.5117 4.4018 -4.4553)	$(0\bar{1}1)$ 5.22° 1.5259
***sip*$_4$**	(2.6790 -4.7318 4.6542)	**$(1\bar{1}1)$ 19.91° 0.0059**
Two likely interfaces	**$(11\bar{2}2)_\alpha//(1\bar{1}00)_\omega$; (*sip*$_4$)** $(\bar{1}2\bar{1}0)_\alpha//(1\bar{1}00)_\omega$ (***sip*$_2$**)	(a) and (b) in Figure S5
Atomic HP	$(11\bar{2}2)_\alpha//(1\bar{1}00)_\omega$	
OR	$(11\bar{2}2)_\alpha//(1\bar{1}00)_\omega$; $[1\bar{1}00]_\alpha//[11\bar{2}0]_\omega$	

*(hkl) is with respect to the lattice from the P-I pathway, not the conventional Bravais lattice.

Part 5. Heterophase junctions in superlattice (HJ-I to HJ-VI in Table 1)

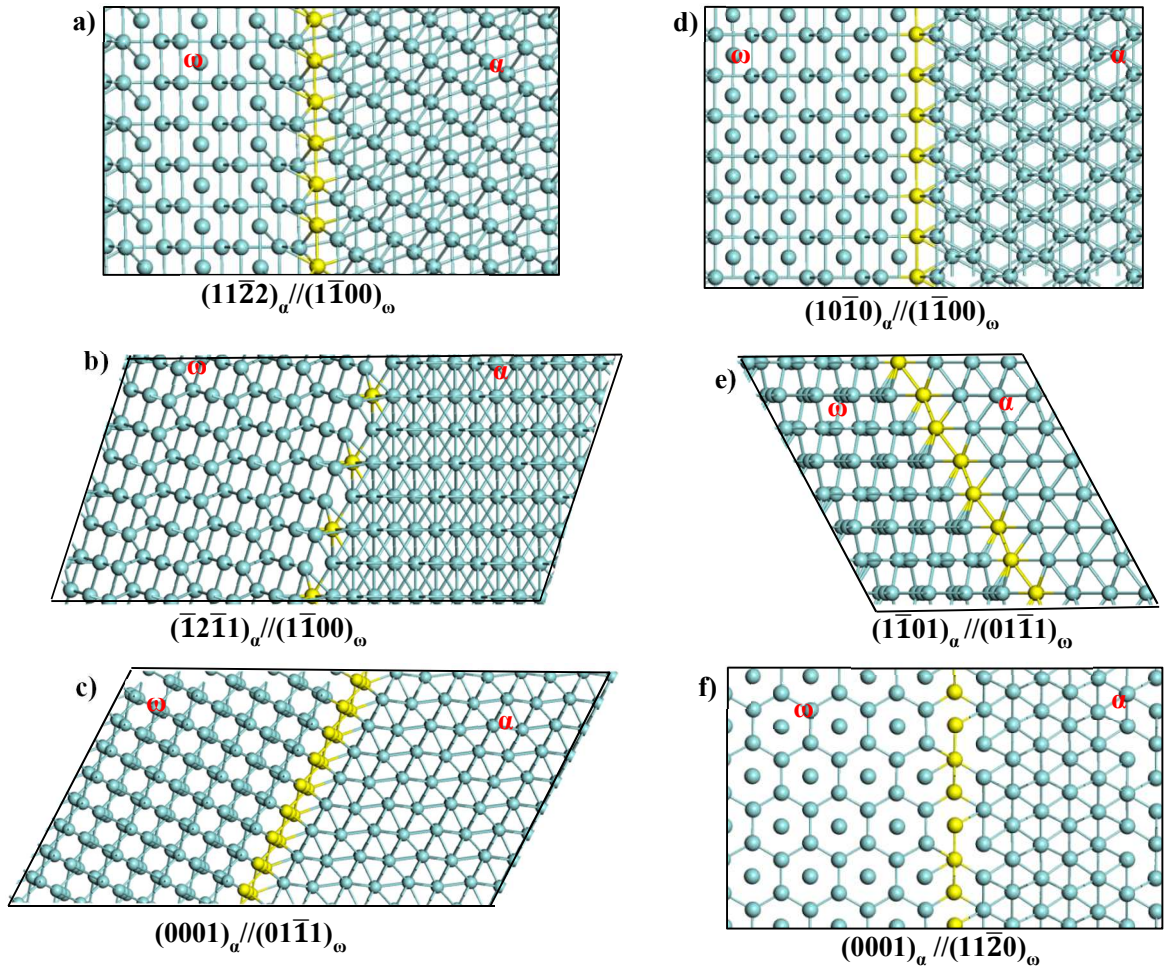

Figure S5. Six possible α-ω heterophase junctions (HJ) created from P-I (a-c) and P-II (d-f). (a) $(11\bar{2}2)_\alpha//(1\bar{1}00)_\omega$ (the most stable interface of P-I, HJ-I, also see Figure 2c; (b) $(\bar{1}2\bar{1}1)_\alpha//(1\bar{1}00)_\omega$; (c) $(0001)_\alpha//(01\bar{1}1)_\omega$(interface suggested from the first condition of Tao-1 OR); (d) $(10\bar{1}0)_\alpha//(1\bar{1}00)_\omega$ (the most stable HJ of P-II, HJ-II, also see Figure 2c; (e) $(1\bar{1}01)_\alpha//(01\bar{1}1)_\omega$ (f) $(0001)_\alpha//(11\bar{2}0)_\omega$(interface suggested from the first condition of Silcock OR, HJ-III in Figure 2c) at hydrostatic pressure of 3 GPa. From our DFT calculations using the superlattice approach, the interface (a), (d-f) can be optimized as stable interfaces with mixed phases, and the other interfaces are not stable, falling back to pure phases after optimization. The calculated interfacial energy is 20 meV/ Å^2 for the HJ-I in (a), 4 meV/ Å^2 for the HJ-II in (d), 33 meV/Å^2 for the interface in (e) and 8 meV/Å^2 for the HJ-III in (f). The interfacial atoms are yellow colored.

The interfacial energy γ_{int} is calculated using Eq. S4.

$$\gamma_{int} = [E(\text{biphase}) - \Sigma_i\, n_i\, E_i(\text{pure phase})]\ /2A \qquad \text{(S4)}$$

where E(biphase) is the total energy of the biphase crystal (superlattice), E_i(pure phase) is the energy of pure phase, n_i is number of Zr of the different phase components in the biphase and A is the surface area of the interface. Obviously, the lower γ_{int} is, the more stable the interface will be. In this work, all the interfaces in superlattice contain the same number of atoms in α and in ω phase (half-half composition).

In Table SIV, we listed the calculated elastic constants of pure α, ω phases, and the heterophase junctions, HJ-I and HJ-II in superlattice (Figure 2c). In general, our DFT results agree with the experimental values and the previous calculations at zero pressure for pure phases. The B/G ratio is related to the brittleness (ductility) of material. A large B/G value indicates a high ductility, while a low value reflects the brittleness. It is seen from Table SIV that the HJ-I from P-I (OR-I, Figure 2c and Figure S5-a) has a larger B/G value than pure α and ω phase, while HJ-II from P-II (OR-II, Figure 2c and Figure S5-d) has a smaller B/G value than pure phases. It shows that HJ-II from P-II would be more brittle than pure zirconium.

Table SIV: Bulk modulus (B), shear modulus (G) and B/G ratio for pure α, ω phase and the mixed phase junctions of zirconium at 3 GPa.

		B	G	B/G
Pure α	This work (3GPa)	102.6	38.2	2.69
	This work (0GPa)	97.4	34.1	2.85
	Expt.	97.6[36] 94[37] 95.3[38]	36.1[38]	
	Other works (0GPa)	93.4[39] 97.1[40] 99.8[41] 97.5[42]		
Pure ω	This work（3GPa）	104.0	50.5	2.06
	This work（0GPa）	97.6	45.3	2.15
	Expt	90.0[37] 109.0[37] 104.0[43]	45.1[43]	
	Other works (0 GPa)	101.1[39]		
HJ-I (Fig. 2)	This work (3GPa)	96.6	28.8	3.35
HJ-II (Fig. 2)	This work (3GPa)	108.0	53.4	2.02

References

1 M. P. Usikov and V. A. Zilbershtein, *Phys. Stat. Sol. (a)*, 1973, **19**, 53-58.

2 A. Rabinkin, M. Talianker and O.Botstein, *Acta Metall*, 1980, **29**, 691-698.

3 A. R. Kutsar, I. V. Lyasotski, A. M. Podurets and A. F. Sanches-bolinches, *High Pressure Res*, 1990, **4**, 475-477.

4 S. G. Song and G. T. Gray, *Philos. Mag. A*, 1995, **71**, 275-290.

5 G. Jyoti, K. D. Joshi, S. C. Gupta and S. K. Sikka, *Philos. Mag. Lett*, 1997, **75**, 291-300.

6 D. R. Trinkle, R. G. Hennig, S. G. Srinivasan, D. M. Hatch, M. D. Jones, H. T. Stokes, R. C. Albers and J. W. Wilkins, *Phys. Rev. Lett*, 2003, **91**, 025701-025704.

7 E. Cerreta, G. T. Gray, R. S. Hixson, P. A. Rigg and D. W. Brown, *Acta Mater*, 2005, **53**, 1751-1758.

8 G. Jyoti, R. Tewari, K. D. Joshi, D. Srivastava, G. K. Dey, S. C. Gupta, S. K. Sikka and S. Banerjee, *Defect Diffus. Forum*, 2008, **279**, 133-138.

9 H. R. Wenk, P. Kaercher, W. Kanitpanyacharoen, E. Zepeda-Alarcon and Y. Wang, *Phys. Rev. Lett*, 2013, **111**, 195701-195705.

10 H. Zong, T. Lookman, X. Ding, S.-N. Luo and J. Sun, *Acta Mater*, 2014, **65**, 10-18.

11 H. Zong, T. Lookman, X. Ding, C. Nisoli, D. Brown, S. R. Niezgoda and S. Jun, *Acta Mater*, 2014, **77**,

191-199.

12 C. Shang and Z. P. Liu, *J.Chem.Theory Comput*, 2013, **9**, 1838-1845.

13 X. J. Zhang, C. Shang and Z. P. Liu, *J.Chem.Theory Comput*, 2013, **9**, 3252-3260.

14 C. Shang, X. J. Zhang and Z. P. Liu, *Phys. Chem. Chem. Phys.*, 2014, **16**, 17845-17856.

15 X.-J. Zhang, C. Shang and Z.-P. Liu, *J.Chem.Theory Comput*, 2013, **9**, 5745-5753.

16 C. Shang and Z. P. Liu, *J. Chem. Theory Comput.*, 2012, **8**, 2215-2222.

17 C. Shang and Z.-P. Liu, *J. Chem. Theory Comput.*, 2010, **6**, 1136-1144.

18 G. Kresse and J. Furthmüller, *Phys.Rev. B*, 1996, **54**, 11169-11186.

19 G. Kresse and J. Furthmüller, *Comput.Mater.Sci*, 1996, **6**, 15-50.

20 P. E. Blöchl, *Phys.Rev. B*, 1994, **50**, 17953-17979.

21 J. P. Perdew, K. Burke and M. Ernzerhof, *Phys.Rev.Lett*, 1998, **80**, 891.

22 G. Kresse, J. FurthmüLler and J. Hafner, *Europhys.Lett*, 1995, **32**, 729-734.

23 W. Frank, C. Elsässer and M. Fähnle, *Phys Rev Lett*, 1995, **74**, 1791-1794.

24 A. Togo, F. Oba and I. Tanaka, *Phys.Rev. B*, 2008, **78**, 134106.

25 Y. Le Page and P. Saxe, *Physical Review B*, 2002, **65**.

26 N. W. Ashcroft and N. D. Mermin, *Philadelphia: Saunders College*, 1976.

27 Z. Sun, S. Li, R. Ahuja and J. M. Schneider, *Solid State Communications*, 2004, **129**, 589-592.

28 E.Schreiber, O.L.Anderson and N.Soga, *New York: Mcgraw-Hill*, 1973.

29 J. S. Bowles and J. K. Mackenzie, *Acta Metall*, 1954, **2**, 129-137.

30 J. K. Mackenzie and J. S. Bowles, *Acta Metall*, 1954, **2**, 138-147.

31 G. K. Bansal and A. H. Heuer, *Acta Metall*, 1974, **22**, 409-417.

32 M.S.Wechsler and T.A.Lieberman, *Trans.Am.Inst.Min.Engrs*, 1953, **197**, 1503-1515.

33 C. M. Wayman, *New York:Macmillan Co.*, 1964, 76-80.

34 C. M. Wayman, *J. Less-Common Metals*, 1972, **28**, 97-105.

35 X. L. Xiao, C. P. Luo and J. W. liu, *Sci. China, Ser. E*, 2002, **45**, 58-64.

36 B. Olinger and J. C. Jamieson, *High Temp.High Pressures*, 1973, **5**, 123-131.

37 Y. Zhao, J. Zhang, C. Pantea, J. Qian, L. L. Daemen, P. A. Rigg, R. S. Hixson, G. T. Gray, Y. Yang, L. Wang, Y. Wang and T. Uchida, *Phys. Rev. B*, 2005, **71**, 184119-184124.

38 E. S. Fisher, *J Appl Phys*, 1970, **41**, 2991.

39 Y. J. Hao, L. Zhang, X. R. Chen, Y. H. Li and H. L. He, *J. Phys. : Condens. Matter*, 2008, **20**, 235230.

40 D. J. OH and R. A. Johnson, *J.Nucl.mater*, 1989, **169**, 5-8.

41 F. Willaime and C. Massobrio, *Phys Rev B*, 1991, **43**, 11653-11665.

42 F. Cleri and V. Rosato, *Phys Rev B*, 1993, **48**, 22-33.

43 W. Liu, B. Li, L. Wang, J. Zhang and Y. Zhao, *Phys Rev B*, 2007, **76**, 144107-144110.

Part 6 The Cartesian atomic coordinates for P-I, P-II, P(HJ-I) and P(HJ-II)

P-I

α-phase a=6.0497 b=5.5458 c=5.5456 α=120° β= 90° γ=117°

X	Y	Z
2.104591	-0.47915	1.909945
0.421708	1.771182	3.438113
4.28239	1.68907	1.146356
1.257478	2.206195	0.381911
3.446659	1.253685	4.202805

	5.129516	-0.9962	2.674263
TS1	a=5.913 b=5.7275 c=5.727 α=124° β= 90° γ=116°		
	X	Y	Z
	2.319818	-0.73684	1.612058
	0.665882	1.855359	3.286472
	4.150509	1.736862	1.350145
	1.216924	1.950416	0.345753
	3.360321	0.752764	4.186863
	5.252898	-0.95056	2.615626
ω-phase	a=5.901 b=5.898 c=5.898 α=130° β= 85° γ=116°		
	X	Y	Z
	2.398665	-0.8832	1.444625
	1.102164	1.764549	2.888627
	4.052608	1.76527	1.444602
	1.102689	1.765681	-0.00052
	3.224138	0.440576	4.334394
	5.348572	-0.88361	2.889734
P-II			
α-phase	a=5.131 b=8.489 c=3.202 α=101° β= 90° γ=90°		
	X	Y	Z
	8.119898	-0.40799	4.546797
	0.436148	9.892251	4.882902
	8.137671	11.72593	0.35479
	8.135627	13.53628	5.594255
	0.44223	13.53678	0.692574
	0.438615	15.34737	5.93141
TS2	a=5.052 b=8.514 c=3.167 α=95° β= 90° γ=90°		
	X	Y	Z
	2.938924	0.539731	1.488119
	0.413742	2.143765	1.714288
	2.938901	3.511379	0.128684
	2.938907	6.116012	2.002049
	0.41379	5.084719	1.198786
	0.413914	16.20388	3.073626
ω-phase	a=5.007 b=8.669 c=3.120 α=90° β= 90° γ=90°		
	X	Y	Z
	7.927614	0.723208	4.679804
	0.417259	10.83581	4.681728
	7.92759	12.2811	1.92E-05
	7.927611	15.17029	4.680914
	0.417247	13.72662	1.55897
	0.417267	16.61582	6.240539
P(HJ-I)	a= 16.475 b= 6.033 c= 5.531 α= 90.7° β= 90.2° γ=83.8°		

α-phase	X	Y	Z
	0.596206	5.440224	5.10589
	0.271105	2.508434	0.447855
	7.234932	3.474308	3.21249
	6.923107	0.477126	2.340986
	5.649523	1.442836	5.105378
	5.981729	4.508243	0.447226
	4.707818	5.472753	3.213205
	4.397375	2.475438	2.34047
	2.777741	0.441366	5.977867
	3.143753	3.509414	-0.42453
	1.869878	4.475319	2.339891
	1.524264	1.475502	3.212639
	8.833636	5.440224	5.10589
	8.508577	2.508434	0.447855
	15.47236	3.474309	3.21249
	15.16053	0.477126	2.340987
	13.88695	1.442837	5.105378
	14.21916	4.508243	0.447225
	12.94525	5.472753	3.213205
	12.6348	2.475438	2.34047
	11.03636	0.509444	0.447026
	11.35999	3.441336	5.106309
	10.10731	4.475319	2.339891
	9.761693	1.475502	3.212639
ts1	a= 17.286 b= 6.142	c= 5.106 α= 90.1°	β= 90.0° γ=90.9°
	X	Y	Z
	-0.07069	5.195743	4.972417
	-0.02198	2.130447	0.157564
	7.102177	3.689735	2.69801
	7.148772	0.619862	2.432735
	5.729693	1.980345	4.973431
	5.685505	5.055846	0.156849
	4.25797	5.2352	2.701828
	4.304609	2.16464	2.428161
	2.876578	0.517628	5.133497
	2.832826	3.593359	-0.0033
	1.358208	5.016387	2.427177
	1.404722	1.94618	2.702846
	8.593499	5.640945	4.885926
	8.642254	2.57586	0.243893
	15.85037	3.492133	2.698005
	15.89735	0.422249	2.4325
	14.35018	1.527956	4.88755

	14.30588	4.603547	0.242974
	12.88758	5.643269	2.815392
	12.93516	2.573375	2.314638
	11.52034	0.516325	0.253651
	11.4724	3.58175	4.87678
	10.02003	4.615441	2.315279
	10.06575	1.544787	2.814879
HJ-I (int1)	a= 17.412 b= 6.165 c= 5.052 α= 90.0º β= 90.0º γ=91.9º		
	X	Y	Z
	-0.16706	5.148065	4.979498
	-0.06644	2.067648	0.093026
	7.082114	3.731736	2.634716
	7.182697	0.651459	2.438065
	5.743924	2.06438	4.980431
	5.643333	5.144336	0.091983
	4.185471	5.199405	2.604972
	4.286242	2.118273	2.467232
	2.890443	0.525514	5.037214
	2.789523	3.60581	0.034915
	1.292942	5.093111	2.466788
	1.393613	2.01239	2.605652
	8.556604	5.663427	4.85557
	8.657447	2.582894	0.217529
	15.91154	3.480148	2.635339
	16.01257	0.399502	2.437487
	14.42754	1.537247	4.855817
	14.32709	4.618039	0.217018
	12.87962	5.669091	2.764449
	12.9804	2.588475	2.308339
	11.59264	0.516747	0.232458
	11.49199	3.597296	4.840311
	10.01588	4.631645	2.309625
	10.11642	1.551017	2.763364
ts2	a= 17.400 b= 6.171 c= 5.046 α= 90.0º β= 90.0º γ=91.8º		
	X	Y	Z
	-0.15543	5.163301	4.98104
	-0.06104	2.079392	0.085442
	7.10411	3.70264	2.618011
	7.19844	0.618721	2.448648
	5.740683	2.05392	4.98425
	5.646086	5.137847	0.082212
	4.195485	5.18983	2.592925
	4.290062	2.105893	2.473472
	2.889992	0.52507	5.028168

	2.795279	3.609112	0.038113
	1.30209	5.112153	2.47122
	1.396579	2.028162	2.595215
	8.55678	5.576777	4.837229
	8.651476	2.492858	0.229743
	15.88992	3.513004	2.622489
	15.98474	0.429052	2.444093
	14.41095	1.599898	4.834134
	14.31659	4.684015	0.232526
	12.88602	5.628995	2.771539
	12.98042	2.545039	2.294927
	11.57544	0.522831	0.210403
	11.48094	3.606733	4.855955
	10.01523	4.718042	2.297718
	10.10937	1.634067	2.768957
int2	a= 17.455 b= 6.223 c= 4.992 α= 90.0º β= 90.0º γ=90.2º		
	X	Y	Z
	17.40834	5.231606	4.954732
	17.41846	2.120001	0.05731
	7.26359	3.652848	2.499564
	7.273555	0.541276	2.513082
	5.811574	2.093888	0.004317
	5.801621	5.205403	0.016236
	4.356819	5.203297	2.512798
	4.366812	2.091798	2.499802
	2.915242	0.526642	0.004289
	2.905277	3.638161	0.016154
	1.470849	5.170609	2.470509
	1.480875	2.059089	2.541748
	8.68752	5.22249	4.972199
	8.697542	2.110774	0.040369
	16.09543	3.591918	2.589427
	16.10549	0.480425	2.42247
	14.47016	1.451376	4.824495
	14.46011	4.562806	0.187544
	13.15713	5.823247	2.684365
	13.16706	2.71167	2.327697
	11.54021	0.568698	0.093417
	11.53014	3.680283	4.918644
	10.20815	5.158287	2.463813
	10.21811	2.046794	2.54851
ts3	a= 17.413 b= 6.216 c= 5.007 α= 90.0º β= 90.0º γ=90.6º		
	X	Y	Z
	17.39039	5.245196	4.969817

	17.40889	2.134749	0.065631
	7.247983	3.667958	2.506872
	7.272801	0.558782	2.527348
	5.800782	2.095989	0.000927
	5.778146	5.20529	0.026081
	4.336782	5.215351	2.528387
	4.359329	2.105794	2.50336
	2.917682	0.534716	0.002618
	2.892658	3.643168	0.023774
	1.44066	5.171654	2.478552
	1.462213	2.06244	2.55659
	8.676365	5.249738	4.981347
	8.697751	2.14066	0.05252
	16.00401	3.596987	2.597801
	16.02785	0.487171	2.438967
	14.49023	1.661456	4.812158
	14.47348	4.771319	0.22352
	13.06037	5.658415	2.726913
	13.08343	2.548262	2.308874
	11.57624	0.612507	0.093039
	11.55443	3.721316	4.942311
	10.14288	5.183737	2.468094
	10.16407	2.075118	2.56772
ω-phase	a= 17.253 b= 6.273	c= 5.013 α= 90.0°	β= 90.0° γ=90.1°
	X	Y	Z
	17.25877	5.242496	5.022379
	17.25679	2.104703	0.009786
	7.193374	3.67192	2.516743
	7.19661	0.534603	2.516118
	5.752437	2.099662	0.010467
	5.749321	5.237213	0.010466
	4.316769	5.242145	2.51594
	4.319908	2.104664	2.515985
	2.880755	0.534325	0.010403
	2.875995	3.670058	0.009885
	1.438831	5.237569	2.51689
	1.443693	2.101905	2.516827
	8.632531	5.242496	5.022379
	8.630553	2.104701	0.009785
	15.81963	3.671919	2.516742
	15.82287	0.534604	2.516118
	14.38564	2.101892	5.023062
	14.37557	5.237214	0.010465
	12.94302	5.242145	2.51594

	12.94616	2.104664	2.515985
	11.50701	0.534326	0.010404
	11.50921	3.672285	5.022479
	10.06509	5.23757	2.516889
	10.06995	2.101904	2.516828
P(HJ-II)			
α-phase	a= 3.204 b= 5.137 c= 16.930 α= 90.0° β= 100.8° γ=90.0°		
	X	Y	Z
	0.004734	3.852591	0.92439
	1.60234	1.284222	1.847286
	0.004613	1.284221	4.619027
	1.611169	3.852589	3.695501
	0.013585	3.852589	6.467223
	1.611165	1.28422	7.390458
	-1.58364	3.852588	9.238135
	0.013948	1.284218	10.16191
	-1.5837	1.284219	12.93352
	0.022808	3.852588	12.01026
	-1.57483	3.852587	14.78185
	0.022666	1.284218	15.70509
ts4	a= 3.160 b= 5.105 c= 17.385 α= 90.0° β= 103.4° γ=90.0°		
	X	Y	Z
	-0.26723	3.813623	0.933973
	1.365899	1.261313	2.032076
	-0.2374	1.260815	4.827882
	1.317172	3.813451	3.730309
	-0.28542	3.812997	6.527409
	1.346479	1.260749	7.626908
	-1.87722	3.813776	9.292987
	-0.22316	1.263229	10.50736
	-1.89731	1.262214	13.27185
	-1.21578	3.814559	12.1669
	-2.88892	3.813547	14.92997
	-1.23324	1.262915	16.14256
HJ-II, int3	a= 3.129 b= 5.087 c= 17.713 α= 90.0° β= 105.4° γ=90.0°		
	X	Y	Z
	-0.37969	3.807248	0.838837
	1.206964	1.263052	2.069911
	-0.38969	1.262304	4.887109
	1.157743	3.806201	3.65027
	-0.42824	3.806118	6.469006
	1.14615	1.262434	7.699129
	-1.98207	3.806149	9.234769
	-0.40322	1.262803	10.64646

	-1.97566		1.263264		13.51695
	-1.95442		3.806455		12.09727
	-3.52096		3.807606		14.96936
	-1.93291		1.261953		16.38112
ts5	a= 3.147	b= 5.047	c= 17.939	α= 90.0°	β= 107.8° γ=97.0°
	X		Y		Z
	-0.26937		3.786473		0.828571
	1.414518		1.262492		2.13233
	-0.20074		1.26299		4.872819
	0.562624		3.786185		3.724435
	-1.05343		3.786882		6.465223
	0.629027		1.263217		7.770206
	-2.56254		3.786744		9.276017
	-0.97524		1.262959		10.67456
	-2.57641		1.263558		13.54806
	-2.56362		3.786924		12.12815
	-4.16372		3.787497		15.00199
	-2.57483		1.263523		16.39955
ω-phase	a= 3.110	b= 5.023	c= 18.146	α= 90.0°	β= 107.2° γ=90.0°
	X		Y		Z
	0.028022		3.764211		0.72929
	1.663281		1.253507		2.1672
	0.243382		1.251384		5.062601
	0.186679		3.763784		3.605641
	-1.23318		3.761712		6.500877
	0.401989		1.249031		7.939045
	-2.6519		3.758874		9.396066
	-1.01699		1.246181		10.83521
	-2.43698		1.244118		13.73083
	-2.49348		3.756518		12.27314
	-3.91364		3.754386		15.1693
	-2.27876		1.243694		16.6084